Am J Cancer Res 2024;14(4):1662-1674
www.ajcr.us /ISSN:2156-6976/ajcr0153948

Original Article

Specific-CT brain template construction and retrospective dosimetric comparison study in brain for nasopharyngeal carcinoma patients treated with IMRT or VMAT

Fenglei Du[1*], Shuang Zheng[2*], Kainan Shao[1,3], Yiwei Yang[1], Wei Chen[1,4], Xue Bai[1], Yonghong Hua[5]

[1]Department of Radiation Physics, Zhejiang Cancer Hospital, Hangzhou Institute of Medicine (HIM), Chinese Academy of Sciences, Hangzhou 310022, Zhejiang, China; [2]School of Media and Design, Hangzhou Dianzi University, Hangzhou 310018, Zhejiang, China; [3]Department of Radiation Oncology, Zhejiang Provincial People's Hospital, Hangzhou 314408, Zhejiang, China; [4]School of Nuclear Science and Technology, University of South China, Hengyang 421001, Hunan, China; [5]Department of Radiation Oncology, Zhejiang Cancer Hospital, Hangzhou Institute of Medicine (HIM), Chinese Academy of Sciences, Hangzhou 310022, Zhejiang, China. [*]Equal contributors.

Received October 16, 2023; Accepted March 12, 2024; Epub April 15, 2024; Published April 30, 2024

Abstract: The current Radiotherapy (RT) technology still inevitably irradiated normal brain tissue, causing implicit radiation-induced injury. This study investigates the precise localization and the corresponding radiation dosage of brain regions susceptible to damage in nasopharyngeal carcinoma (NPC) patients following RT. Utilizing the Advanced Normalization Tools (ANTs) package, a computed tomography (CT) brain template was created in the standard Montreal Neurological Institute (MNI) space, based on 803 Chinese NPC patients (T0~T4) who underwent RT. With this template, all patients' CT and RTdose data were registered to the MNI space, and the RTdose distribution characteristics in normal brain tissues were compared for NPC patients treated with Intensity-modulated radiotherapy (IMRT) or Volumetric Modulated Arc Therapy (VMAT), with patients' age and gender as covariates. Analysis of the average dosages indicated that certain areas within the Limbic, Temporal, and Posterior Lobes, the Brainstem, and the Cerebellum Posterior Lobe were exposed to doses exceeding 50 Gy. Inter-group analysis revealed that IMRT delivered higher doses than VMAT to brain regions anterior to the nasopharyngeal tumor, whereas VMAT affected the posterior regions more. Interestingly, VMAT showed a drawback in preserving the normal brain tissues for T4-stage patients. This revealed that the two treatment modalities have unique characteristics in preserving normal brain tissue, each with advantages. With better localization precision, the created CT brain template in MNI space may be beneficial for NPC patients' toxicity and dosimetric analyses.

Keywords: Population-specific CT brain template, nasopharyngeal carcinoma, IMRT, VMAT, dosimetry

Introduction

Nasopharyngeal carcinoma (NPC) is a common endemic cancer frequently occurring in the head and neck region with a distinct geographical distribution and high prevalence in Southeast Asia [1, 2]. NPC is a type of cancer that is very sensitive to radiation therapy (RT) [2]. Because of its deep-seated location in the body and its high sensitivity to radiation, RT is the most common form of treatment for NPC [3, 4].

Damage to normal tissues from RT may arise when striking a balance between optimal tumor exposure and adhering to dose limits for critical organs poses a challenge (OARs). Brain tissues near the nasopharyngeal tumor are vital areas that could be easily affected by RT. Recently, RT-induced brain necrosis has been increasingly studied with increased survival rates and positive outcomes in patients with NPC [5-8].

Numerous research studies have looked into the structural or functional problems that RT

https://doi.org/10.62347/HACN9549

causes in survivors of NPC. These include changes in the gray matter [9, 10], hippocampal atrophy [11], and cognitive impairments [5, 7, 12, 13].

However, limited publications have addressed the explicit correlation between the structural or functional abnormalities, the associated cognitive impairments, and the corresponding radiation doses. This may be due to the difficulty in precisely corresponding and elaborating the detailed location of the irradiated structure, the dose accepted by the specific structure, and the corresponding cognitive function of the location.

Thankfully, voxel-based (VB) techniques emerged within the realm of radiation oncology in recent years, inspired by the successful application of neuroimaging methods. This innovative approach has offered a new solution to address these challenges [14]. The use of VB morphometry has demonstrated its utility in examining the pathophysiological changes associated with various neuroinflammatory and neurodegenerative disorders. The backbone of a VB analysis is a spatial normalization of various anatomies to a common coordinate system (CCS). The most widely used CCS in neuroimaging is the Montreal Neurological Institute (MNI) coordinate system [15-20]. Besides, in order to determine the radiation dose of radiotherapy in the Treatment Planning System (TPS) based on the computed tomography (CT) electron density, CT imaging was essential and predominant for NPC patients. Thus, we need a standard brain template in CCS based on CT modality to conduct the VB analysis for NPC patients.

Brain templates generated using in CT images are rarely documented in the literature. One study introduced an axial CT template designed for a group of individuals who had experienced a stroke, derived from a sample of 35 healthy elderly individuals [21]. A bimodal MR-CT (Magnetic resonance - CT) brain template was developed for neonates whose gestational age ranged from 39 to 42 weeks [22]. An age-specific non-contrast CT atlas with great resolution was created for the elderly by Deepthi Rajashekar et al. [23]. From the CQ500 dataset - a public available collection of non-contrast brain CT scans of patients with symptoms of head trauma or stroke provided by (qure.ai, http://headctstudy.qure.ai/dataset) [24] - John Muschelli [25] constructed a high-resolution unbiased CT template. As far as we aware, no generic CT brain template that works well for Chinese patients with NPC has been described.

Furthermore, it has been observed that Asian and Caucasian brain traits differ significantly [17, 26-28]. Prior research has demonstrated that, in comparison to population-specific templates, applying the template developed using adult participants from North American or Western European people to Chinese results in more severe deformation and decreased consistency [26-28]. Moreover, the accuracy of brain segmentation and registration was influenced by the gender, age, sample size, and ethnicity of the template. When mismatched templates were employed in the spatial normalization process, the performance of the brain segmentation and registration of the brain dramatically declined [27-29]. Thus, a population-specific CT template that takes into account factors like age, ethnicity, and nationality should be used to improve the precision and quality of segmentation and registration for Chinese NPC patients.

Therefore, we created a specific axial CT brain template in the standard MNI space based on a rich data set of NPC patients, and the detailed location of the irradiated brain structure and the dose accepted by the specific structure for NPC patients after RT were explored. Using this particular CT brain template, the precise normal brain areas were identified, the dose distribution in these locations was shown, and the dosimetry features of certain normal brain areas of patients with NPC treated with various RT methods were examined. The present study provided a more intuitive way of evaluating the brain irradiation characteristics of NPC patients following RT.

Materials and methods

The Zhejiang Cancer Hospital's institutional ethical review committee gave its approval to our investigation. All NPC patients signed informed consents upon admission to the hospital, agreeing to allow their clinical data to be used for non-profit scientific research.

Table 1. Demographic characteristics of 803 patients

		T categories				
		T0	T1	T2	T3	T4
Number		1	81	98	416	207
Gender	Male	-	61	61	294	151
	Female	1	20	37	122	56
Age (Y)	Median age	55	55	51	52	55
	Range	-	28~77	26~77	18~80	25~84
Radiotherapy	IMRT	-	57	66	245	129
	VMAT	1	24	32	171	78
Nasopharynx RT dose (Gy)		70.4	70.5 (67.2-73.6)	70.6 (69-72.6)	70.4 (69-72.6)	70.4 (66.9-74.2)
CT scanner	GE	-	48	50	211	110
	Philips	1	33	48	205	97

IMRT: Intensity-modulated radiotherapy; VMAT: Volumetric Modulated Arc Therapy.

Participants

A retrospective analysis was carried out on 803 patients who were hospitalized to our clinic between December 2014 and November 2019 with newly diagnosed NPC. Only patients who had CT scans encompassing the whole brain range were included.

The exclusion criteria were as follows: significant previous head trauma, substance or psychoactive drug abuse in the present or past, neurological or psychiatric disorders, viral hepatitis, other severe systematic diseases, other brain tumors, distant metastases in brain and other major medical illness affected the patient's prognosis.

Table 1 details characteristics of 803 patients. These patients had a median age of 53 years, ranging from 18 to 84 (567 males). The 7th edition of the International Union against Cancer/American Joint Committee (UICC/AJCC) staging system was used to categorize the clinical T stages for patients with NPC. Tumors were classified as T0 in one case, T1 in 81 cases (61 males), T2 in 98 cases (61 males), T3 in 416 cases (294 males), and T4 in 207 cases (151 males).

CT data acquisition

All CT images were obtained within the context of routine clinical condition using either a Philips or a GE CT scanner specified for RT. In the supine position, patients were rendered immobile with a thermoplastic mask. High-resolution CT images were acquired in the GE CT scanner with a 2.5 mm or 5 mm slice thickness, or in the Philips CT scanner with a 3 mm or 5 mm slice thickness. All CT images were enhanced with contrast when acquired. These images of patients were first checked by visual inspection. Only patients whose scans covered the total brain volume were enrolled in the present study.

Radiotherapy

For OAR and target volume delineation, all patients' CT scans were sent to the TPS (Raystation 4.5, RaySearch Laboratories, Sweden). Radiation oncologists defined target volume and OARs for each patient slice-by-slice on contrast-enhanced CT scans in accordance with guidelines provided by the International Commission on Radiation Units and Measurements (ICRU) 50 [30] and 62 reports [31]. The contouring of patient targets involved the expertise of multiple clinicians, and the study's robust sample size allowed for the mitigation of individual differences in target delineation to an extent where they could be minimized to a very low level, if not entirely overlooked. Target volumes include GTVnx (the gross tumor within the nasopharynx), and GTVnd (the gross nodal target in the neck). The clinical target volume (CTV) includes CTV1 (high-risk region), and CTV2 (the preventive region). The planning target volumes (PTVs) were created by extending 3 mm around the GTV or CTV in the TPS through margin expansion. OARs were contoured according to the ICRU 83 report [32] for dose constraint evaluation.

The PTV of GTVnx was administered with a dosage of 67-74 Gy in 30-33 fractions, while the PTV of GTVnd was given 60-74 Gy, the PTV of

CTV1 was given 60-64 Gy, and the PTV of CTV2 was given 52-56 Gy. Patients were delivered one fraction/day for 5 days per week. All PTVs were radiated within a simultaneous integrated boost (SIB) plan.

Using an Elekta (Elekta Synergy) or Varian (Varian 23EX or Trilogy) linear accelerator, patients received treatment using either volumetric modulated arc therapy (VMAT) or intensity-modulated radiation therapy (IMRT). The Raystation TPS is where the IMRT and VMAT RT plans were produced. Seven or nine static coplanar fields (equally spaced at 52° and 40°) of six-MV X-rays, were used for IMRT plans. Two or four revolving arcs of the same energy were set for VMAT plans, ranging from 178° to 182° counterclockwise and from 182° to 178° in clockwise direction. For all targets, the overall clinical goal was to achieve at least 95% of prescription doses to planned targets. Each OAR's dose was limited in accordance with the ICRU 83 report [32] and RTOG 0225 protocol [33]. All plans were evaluated and approved by physicians before delivering to patients.

CT template construction

All CT brain scans of NPC patients involved in this study were used to develop a novel population-specific brain template in CT modality. In the current work, template construction techniques that have been used and verified in the past [21, 34] were adopted, such as nonlinear registration and transformation.

Using 3D Slicer software [35], all CT scans and their associated RT dose distribution images (RTdose images) were first cropped to eliminate surplus information in the vicinity of the head simultaneously. These cropped images were then manually transformed to align to the anterior commissure - posterior commissure line (AC-PC line) with Statistical Parametric Mapping 8 (SPM8, http://www.fil.ion.ucl.ac.uk/spm/software/spm8/). As a result, there was a coarse alignment between the CT scans (together with corresponding RTdose images) and the MNI template. It is difficult to register CT scans directly to the magnetic resonance imaging (MRI) MNI152 template because the soft tissues of the brain on such images lack sufficient contrast. Therefore, an invertible formula was used to convert the CT image intensity from Hounsfield Units (HU) to more precisely distinguish cerebral soft tissues that show poor contrast on original CT images [21]. The CT image intensities were converted in the following ways: values greater than 100 were converted to i+3000, values between -99 and 100 were linearly scaled to the range 901 to 3100, and values between -1000 and -100 were translated to 0 to 900.

The 'coregister' and 'normalise' functions of SPM8 were used to linearly align CT images with 12 parameters (translations, rotations, zooms, and shears, each in three dimensions) to the MNI152 template. Images were resliced to a 1×1×1 mm resolution with a broad bounding box (XYZ min; max [-90 -126 -82; 90 90 108]) using the third-degree b-spline interpolation. The Advanced Normalization Tools (ANTs, http://stnava.github.io/ANTs/) package [36] was then adopted for template construction. The 'antsMultivariateTemplateConstruction2.sh' script in the ANTs package was executed. The iteration number was set by default to 4 and the affine average of all the images was set as an unbiased starting point. Other parameters were set by default. The output of this first in ANTs was transferred to MNI space utilizing SPM8's 'coregister' and 'normalise' function with a bounding box ([-90 -126 -72; 90 90 108]). The 'antsMultivariateTemplateConstruction2.sh' script was then re-run on the same CT images but now with this newly transferred image as the target of all inputs. Parameters were set the same as the first run, except 'a' (image statistic used to summarize images) as 0 to retain the accurate average HU values for all voxels. The resulting image was the CT brain template in asymmetric MNI space, with which individual CT and RTdose images can be registered into the uniform MNI space and group statistics can be performed.

Statistical analysis

Patients' CT images and matching RTdose maps were first transformed to the template constructed here with a resolution of 2×2×2 mm synchronously. SPM8 was utilized to conduct all registrations. The group-wise analysis was executed for the registered RTdose images in the MNI space.

One patient was classified as T0 stage and thus excluded from the group-wise analysis. Using SPSS software (version 20), a statistical study

of the descriptive features of patients with various T stages was carried out. The Shapiro-Wilk test verified the normality of the quantitative variable (age). In the event that the age was not normally distributed, the Wilcoxon test was utilized to compare the mean age. In all other cases, the ANOVA test was used. It was determined to be statistically significant when $P < 0.05$. To evaluate the differences between patients' various T stages, the chi-square analysis was employed to examine the gender and RT techniques, using a *p*-value of less than 0.05 as the threshold for statistical significance.

Patients' RTdose images were firstly averaged for each radiotherapy technique (RTtech, including IMRT and VMAT) within the dpabi toolbox [37]. The average RTdose images were projected onto the Colin27 MRI brain surface template to depict the overall distribution of doses in brain. To better illustrate the distribution of doses within the brain, we have separately displayed the distributions of doses > 1.0 Gy, > 30 Gy, and > 50 Gy. This selection was made only to enhance the clarity and visualization of radiation distribution, allowing for a more comprehensible interpretation of the data.

Then, using the "statistical analysis" function in the dpabi toolbox [37], the VB analysis of dosimetric properties of various RTtechs in the brain was investigated in 2-sample t-tests, employing a permutation threshold-free cluster enhancement (TFCE) test (permutation number = 5000, FWE $P < 0.05$) for each T stage of patients as well as for all patients. The variables of age and gender were set as covariates in this test. The MATLAB BrainNet viewer toolbox [38] and the xjView toolbox (http://www.alivelearn.net/xjview) were adopted to display the brain regions where the dose distribution disparities between IMRT and VMAT.

Results

The CT template was constructed on a computer with an AMD R5 3600 8-Core 3.6G Hz CPU and 16G RAM. The first run of the 'antsMultivariateTemplateConstruction2.sh' script in the ANTs package cost 438 h 12 m 5 s, and the second run cost 423 h 12 m 55 s. The registration of a single patient's CT (together with its corresponding RTdose images) to the constructed CT template produced for NPC patients is demonstrated as an example in **Figure 1**.

The age distribution of patients with varying T stages (T1, T2, T3, and T4) was examined using the Shapiro-Wilk test. Our findings demonstrated that all T1 to T4 stages had *P*S > 0.05 (T1: $P = 0.333$; T2: $P = 0.896$; T3: $P = 0.214$; T4: $P = 0.40$), suggesting that the variable of age was distributed normally for patients in all stages. After that, the age difference between the various T stages of patients was investigated using a one-way ANOVA. The results showed that there was a significant variation between the T stages ($F(3,801) = 2.812$, $P = 0.038$). Only the difference in the patient's age between the T3 and T4 stages was significant, according to the results of the Bonferroni post hoc test ($P = 0.045$). The age variable of all patients was found to be non-normally distributed ($P = 0.015$) by the Shapiro-Wilk test. Thus, the nonparametric Kruskal-Wallis test was applied to compare the differences of ages for 4 stages of patients. A very similar outcome was discovered: there was a significant difference ($P = 0.041$) among the four T stages. Only the difference between the T3 and T4 stages in patients' ages was significant, according to a subsequent nonparametric analysis ($P = 0.01$). The chi-square analysis revealed that neither gender nor RT techniques among the four T stages of patients were statistically significant (*PS* > 0.01).

The group-wise analysis of dosimetry features used age, gender, and RT techniques as covariates, despite the fact that some of them did not differ significantly among stages.

Average of RTdose images

By averaging patients' RTdose images of each patient for each RTtech, the preview of RTdose images was generated. The preview images were then mapped onto the Colin27 MRI template in the BrainNet viewer toolbox [38]. To illustrate the brain regions accepted relatively higher doses (doses more than 30 Gy and doses more than 50 Gy) during RT, regions covered by the > 30 Gy and > 50 Gy dose distribution maps are also illustrated (**Figure 2**).

To illustrate the regions accepted relatively higher doses (doses more than 50 Gy) during RT, the locations of brain areas that received

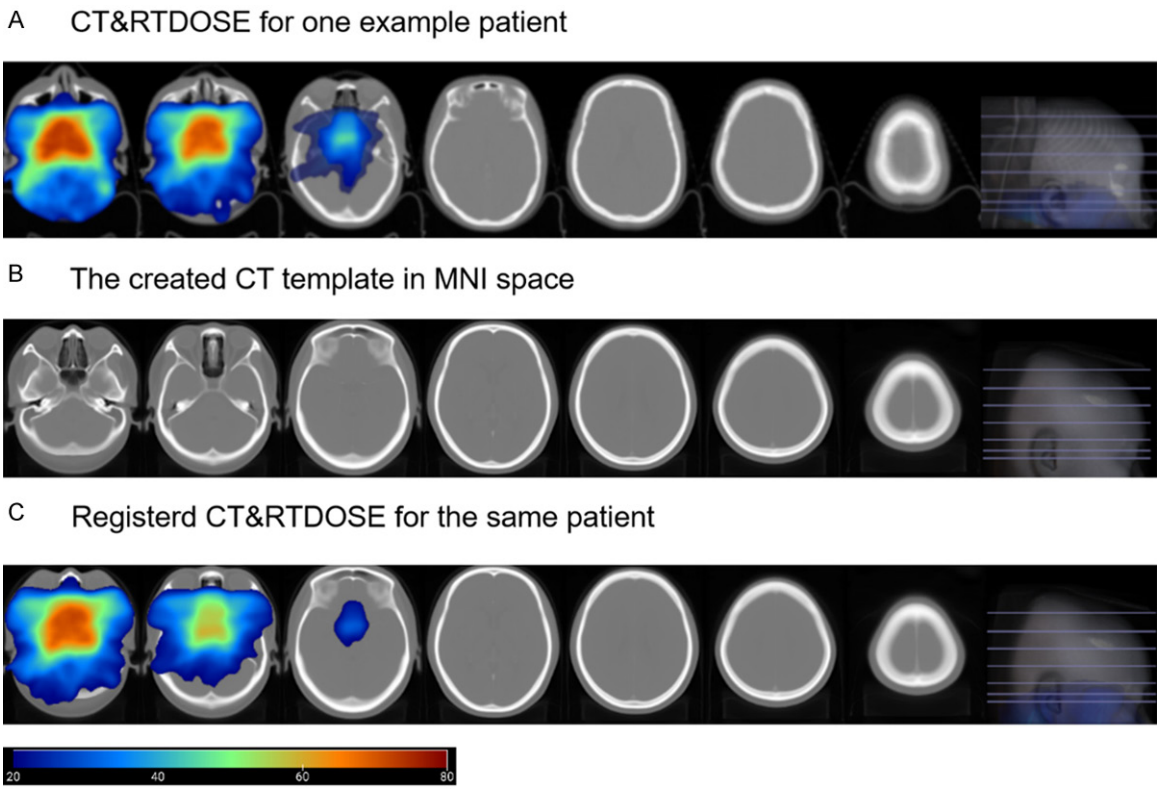

Figure 1. Slices of the CT and RTDOSE images for a single example patient are displayed in (A); slices of the constructed NPC CT template are displayed in (B) in the MNI space; and slices of the CT and RTDOSE images are registered to the constructed NPC CT template for the same patient are displayed in (C). The regions where dose > 20 Gy were displayed in the RTDOSE images. CT: computed tomography; RTDOSE: radiotherapy dose; NPC: nasopharyngeal carcinoma; MNI: Montreal Neurological Institute.

doses more than 50 Gy were reported in **Table 2**. The Limbic and Temporal Lobe, the Brainstem, and a portion of the Cerebellum Posterior Lobe were among the brain regions where patients receiving IMRT and VMAT treatments received doses more than 50 Gy. The result showed that brain regions that received doses of more than 50 Gy in patients treated by IMRT and VMAT were very similar. The detailed sub-brain regions of these areas are shown in Supplementary File.

Variations in RTdose images between IMRT and VMAT RTtechs

Figure 3A displays group variations of RTdose data for all patients treated with different RTtechs.

Brain areas that received less dose in patients undergoing IMRT than those undergoing VMAT located in the Cerebellum Posterior and Anterior Lobe, the Occipital, Temporal, Frontal and Limbic Lobe, the Brainstem, and the Sub-lobar. Brain areas that received more dose in patients undergoing IMRT method than those undergoing VMAT were located in the Temporal, Frontal, Limbic and Occipital Lobe, the Brainstem, Sub-lobar, and a little part of the Cerebellum Anterior Lobe. The detailed sub-brain regions of these areas are shown in Supplementary File. **Table 3** lists the voxel sizes, peak T values, and the peak values' locations in MNI space for all brain areas.

There was no significant difference between the RTdose data for T1 patients treated with different RTtechs.

Figure 3B displays group variations in RTdose data for patients of T2 stage treated with different RTtechs.

Brain areas that received more dose in patients undergoing IMRT than those undergoing VMAT were located in the Frontal, Temporal, Parietal and Limbic Lobe, the Brainstem, Sub-lobar and the Cerebellum Anterior Lobe. Brain areas

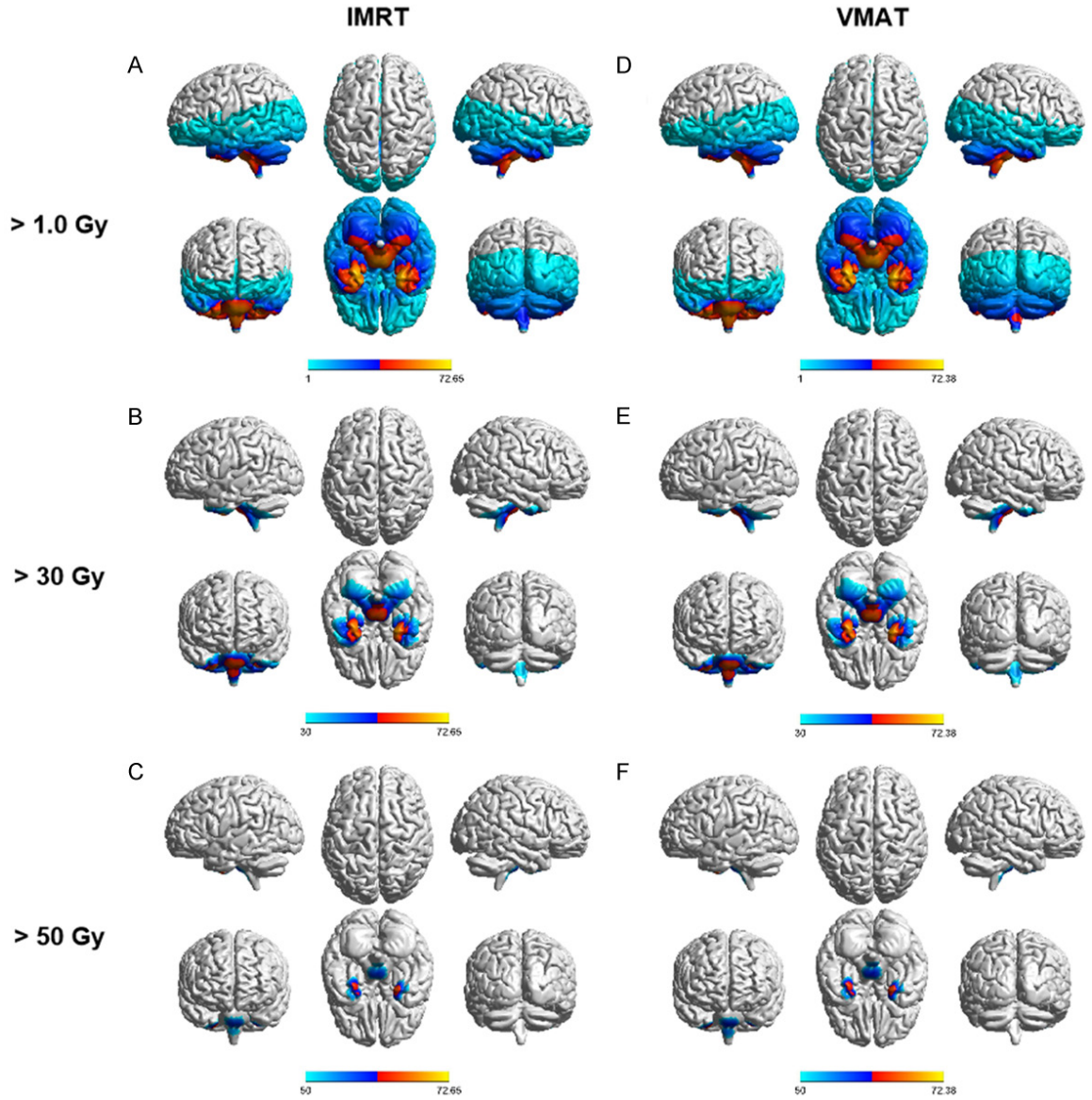

Figure 2. The overview of average subranges' RTdose maps projected into ICBM 152 template. Patients treated by IMRT (497 patients) are shown in (A-C); patients treated by VMAT (306 patients) are shown in (D-F). The thresholds for the dose display range were > 1.0 Gy (A, D), > 30 Gy (B, E), and > 50 Gy (C, F). Note: '> 1.0 Gy' signifies that only the regions where the average dose exceeds 1.0 Gy are displayed; '> 30 Gy' signifies that only the regions where the average dose exceeds 30 Gy are displayed; '> 50 Gy' signifies that only the regions where the average dose exceeds 50 Gy are displayed. RTdose: radiotherapy dose; ICBM: International Consortium for Brain Mapping; IMRT: Intensity-modulated radiotherapy; VMAT: Volumetric Modulated Arc Therapy.

received less dose in patients undergoing IMRT than those undergoing VMAT were located in the Cerebellum Posterior Lobe and a bit of the Brainstem. The detailed sub-brain regions of these areas are shown in Supplementary File. Table S1 lists the voxel sizes, peak T values and the peak values' locations of all brain regions mentioned above.

Figure 3C displays group variations in RTdose data for patients of T3 stage treated with different RTtechs.

Brain areas that received more dose in patients undergoing IMRT than those undergoing VMAT were located in the Temporal, Frontal, Limbic and Occipital Lobe, the Brainstem, Sub-lobar

Table 2. The locations of brain areas that received doses more than 50 Gy in patients treated by IMRT and VMAT, voxel size: 2×2×2

Regions	Sub Regions	Voxel size	Peak Dose value (Gy)	MNI coordinate		
				x	y	z
IMRT						
Limbic Lobe	Uncus	416	67.41	-26	2	-50
Temporal Lobe	Inferior Temporal	137	64.73	-30	0	-50
	Superior Temporal	142	65.20	-24	6	-46
	Middle Temporal	67	62.03	-32	2	-50
	Sub-Gyral	67	60.60	-26	8	-44
Brainstem	Pons	252	65.16	6	-16	-42
	Medulla	123	66.05	6	-20	-46
Cerebellum Posterior Lobe	Cerebellar Tonsil	208	61.97	26	-34	-52
VMAT						
Limbic Lobe	Uncus	381	68.11	-26	2	-50
Temporal Lobe	Inferior Temporal	138	65.87	-30	0	-50
	Superior Temporal	130	66.05	-26	6	-48
	Middle Temporal	68	63.47	-32	2	-50
	Sub-Gyral	65	61.24	-26	8	-44
Brainstem	Pons	243	66.05	-6	-16	-42
	Medulla	141	67.48	-6	-20	-46
Cerebellum Posterior Lobe	Cerebellar Tonsil	261	63.29	26	-34	-52

IMRT: Intensity-modulated radiotherapy; VMAT: Volumetric Modulated Arc Therapy; RTtechs: radiotherapy techniques; MNI: Montreal Neurological Institute; FWE: family-wise error.

and a little part of the Cerebellum Anterior Lobe. Brain areas that received less dose in patients undergoing IMRT than those undergoing VMAT were located in the Cerebellum Posterior and Anterior Lobe, the Occipital Lobe and the Brainstem. The detailed sub-brain regions of these areas are shown in Supplementary File. Table S2 lists the voxel sizes, peak values, and the peak values' locations of all brain regions mentioned above.

Figure 3D displays group variations in RTdose data for patients of T4 stage treated with different RTtechs.

No specific brain regions were found where the dose given to individuals receiving IMRT was significantly higher than that given to those receiving VMAT. Brain areas that received less dose in patients undergoing IMRT than those undergoing VMAT were located in the Cerebellum Posterior and Anterior Lobe, the Occipital, Temporal, Frontal and Limbic Lobe, the Brainstem and a bit of the Sub-lobar. The detailed sub-brain regions of these areas are shown in Supplementary File. Table S3 lists the voxel sizes, peak T values, and peak values' locations of all brain regions mentioned above.

Discussion

Herein, our first objective in this study was to create a CT brain template for normalizing CT images, as CT was the requisite and dominant modality for NPC patients treated with RT. Global variations in brain shape, volume and size between Chinese and Caucasian people have been documented in earlier research [17, 26, 27]. A sample size of 200 images was adequate for creating a template of brain, according to Guo-Yuan Yang [27]. Compared to CT templates of previous studies, our sample size was much larger. For instance, 35 elderly, healthy people served as the basis for the axial CT template constructed by Christopher Rorden et al. [21]. Based on 26 infant CT scans, Sona Ghadimi et al. [22] created a bimodal MR-CT head template. The non-contrast CT atlas generated by Deepthi Rajashekar et al. [23] comprised of 47 patients. The high-resolution unbiased CT template created by John Muschelli [25] was based on 130 patients. This study used 803 Chinese NPC patients' CT brain images to construct an MNI space template. This endowed our CT template with higher stability than those created in previous studies. Furthermore, the CT templates mentioned

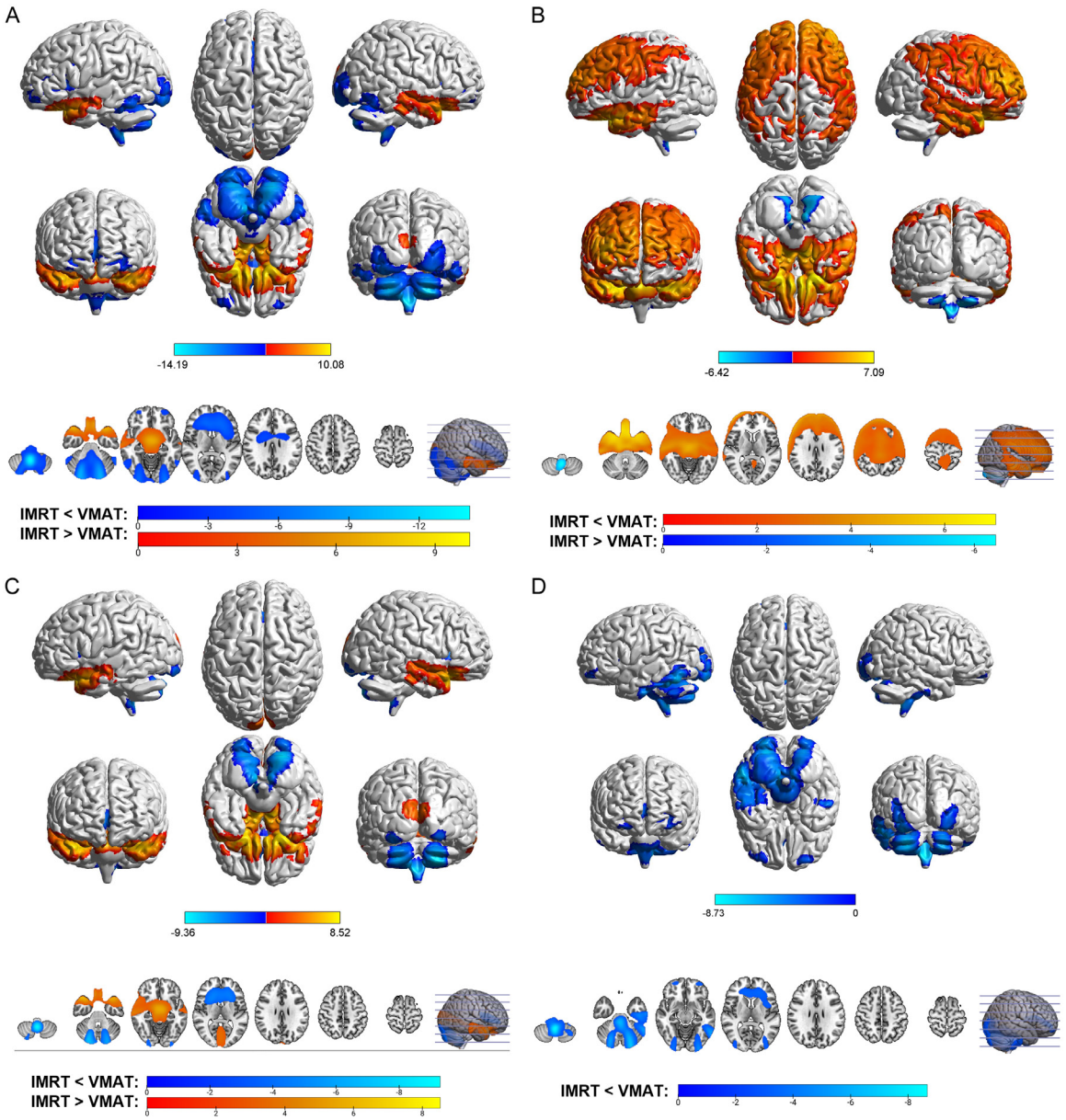

Figure 3. An overview of the variations in RTdose between individuals receiving VMAT versus IMRT (TFCE test, FWE $P < 0.05$). A. The image shows the projection of the result of all patients (IMRT vs. VMAT) into the ICBM 152 template, in the view of surface and transverse section. B. The image shows the projection of T2-stage patients. C. The image shows the projection of T3-stage patients. D. The image shows the projection of T4-stage patients. RTdose: radiotherapy dose; TFCE: threshold-free cluster enhancement; IMRT: Intensity-modulated radiotherapy; VMAT: Volumetric Modulated Arc Therapy; MRI: Magnetic Resonance Imaging; FWE: family-wise error.

above in the literature were generated from a specific cohort of the population, such as the olds [21], the newborns [22], the ischemic stroke patients [23], and the population from a publicly available CT data source without any demographic details [25]. Compared to them, our template was derived from a particular cohort of Chinese NPC patients, which made it more suitable for RT-related research with NPC patients in China and Southeast Asia.

Using this CT brain template will make it possible and more convenient for researchers to explore how radiation changes the structure and function of the brain. In our present study, we registered all patients' RTdose data to the created CT template and averaged the dose distribution maps for different RTtechs of patients. Based on the projection of average RTdose maps onto the International Consortium for Brain Mapping (ICBM) 152 template (**Figure**

Table 3. Brain regions showed variations in RTdose between individuals receiving VMAT versus IMRT (FWE P < 0.05), sample size: 2×2×2, voxel size > 30

Regions	Voxel size	Peak T value	MNI coordinate		
			x	y	z
IMRT < VMAT					
Cerebellum Posterior Lobe	9479	-14.06	2	-52	-52
Frontal Lobe	6664	-6.04	14	38	2
Occipital Lobe	4970	-8.31	24	-88	-26
Sub-lobar	4545	-10.32	0	-52	-44
Cerebellum Anterior Lobe	1892	-8.03	-18	-66	-34
Limbic Lobe	1805	-6.00	10	38	2
Temporal Lobe	1299	-6.89	-58	-54	-24
Medulla	353	-13.36	2	-48	-52
Pons	294	-7.15	0	-44	-42
IMRT > VMAT					
Temporal Lobe	5142	8.36	-22	10	-26
Frontal Lobe	3642	9.53	10	12	-24
Limbic Lobe	1777	9.76	-12	0	-22
Midbrain	1444	8.83	4	-10	-20
Sub-lobar	678	6.71	0	-8	-12
Occipital Lobe	246	3.96	2	-96	18
Pons	181	7.57	-6	-10	-24
Substania Nigra	50	6.41	-6	-12	-12
Cerebellum Anterior Lobe	31	3.68	12	-32	-14

IMRT: Intensity-modulated radiotherapy; VMAT: Volumetric Modulated Arc Therapy; RTtechs: radiotherapy techniques; MNI: Montreal Neurological Institute; FWE: family-wise error.

2), we discovered that the brain regions most commonly exposed to high doses (i.e., doses more than 50 Gy) were the Limbic and Temporal Lobe, the Brainstem, and part of the Cerebellum Posterior Lobe. RT-induced brain injury was more likely to occur in these areas because of their vulnerability to RT damage. For example, Cheng-Yun Yao et al. [39] analyzed 327 patients with NPC undergoing IMRT and discovered that 8 had brainstem damage caused by radiation. Xi-Gang Fan et al. [40] discovered that radiation-induced brainstem necrosis was identified in 6 out of 479 NPC patients. The maximum brainstem dose was discovered to be greater in individuals with radiation-induced brainstem necrosis than in those without the condition. Additionally, Sheng-Fa Su et al. [41] discovered a comparatively high rate of temporal lobe damage. These kinds of radiation-induced necrosis could be easily detected and diagnosed. Radiation may potentially cause subtle alterations in the brain that are not detectable using the present clinical standards. For instance, researchers discovered that in NPC patients treated with RT, the diffusion decreased in bilateral cingulate angular bundle fibers overtime during the first year after RT [42]; the progressive structural information of the bilateral temporal lobe changes considerably [9]; also dose the cortical thickness [43]. These minute alterations could lead to cognitive impairment and provide more insight into the pathophysiology of RT-induced cognitive decline. The dose distribution map in our study clearly shows that the majority of the brain areas with structural or functional alterations reported in these studies tended to receive greater radiation doses.

Very few prior studies examined the direct association between specified structural or functional alterations and the relevant dosage that was delivered. Among them, there was only one study that attempted to look into the association between the dosage and the structural information of the hippocampus. The result showed that the mean dose of the ipsilateral hippocampus and volume changes of the bilateral granule cell layer, bilateral hippocampus, and right molecular layer were significantly correlated negatively [11]. The dosage data used in their investigation came from the Dose-Volume Histogram of anatomy of the hippocampus region, which was manually drawn on CT axial images used for treatment planning. While, structures' volumes were generated based on an atlas constructed from postmortem ex vivo MRI data. This strategy did not result in a strict correspondence between the dose information and the hippocampal imaging data. In addition, the process of manually delineating structures takes a great deal of time, and the results obtained by various physicians are not always uniform. The CT template developed in our work might be utilized for transforming the dose distribution map into MNI space, in which there were standard atlases for most brain structures. In this way, making the imaging data of structures properly correspond to their dosage data will be more practical.

With our developed CT template, we also compared the group differences for the RTdose data of various RTtechs. Our findings showed

that, in comparison to VMAT, brain areas receiving more doses with IMRT were primarily distributed in the anterior region close to the nasopharyngeal tumor, whereas brain areas receiving more doses with VMAT (comparing to IMRT) were primarily located in the posterior region close to the nasopharyngeal tumor; In the T1 stage, no significant variation was found between the two RTtechs; In the T2 stage, brain areas that shown notable distinctions between the two RTtechs were broadly distributed, and VMAT demonstrated a notable dosage advantage in preserving normal brain tissues; In the T3 stage, brain areas receiving more doses with IMRT (comparing to VMAT) were primarily located in the anterior region close to the nasopharyngeal tumor (such as the Temporal Pole and the Limbic Lobe), whereas brain areas receiving more doses with VMAT (comparing to IMRT) were primarily distributed in the Cerebellum; In the T4 stage, VMAT demonstrated a drawback in preserving normal brain tissues. This revealed that the two treatment modalities have unique characteristics in preserving normal brain tissue, each with its advantages.

Results from earlier research were not always consistent. For example, Szu-Huai Lu et al. [44] discovered that VMAT offered superior brainstem sparing. A different investigation discovered that VMAT had a lower maximum dose in the temporal lobe [45]. According to Chen et al. [46], the brainstem of the VMAT have a maximum dosage that was greater than IMRT. Our investigation revealed that there were several moving parts in the distinction between VMAT and IMRT. VMAT and IMRT each have their advantages. Compared to IMRT, VMAT does not exhibit a clear-cut benefit in terms of preserving normal brain tissue. Our analytic objects differed from those used in other research. Through simultaneous registration of RTdose images and planning CTs to our constructed CT brain template, the OAR dose was compared voxel by voxel. On the other hand, Maximum doses of the OARs examined in earlier research were obtained from specific areas. This variation led to a range of outcomes. This discrepancy is significant and warrants more investigation.

Our study has certain drawbacks. First of all, the accuracy of registration in Group-Wise analysis will be improved by creating a bimodal MR-CT brain template from the fully aligned MR and CT imaging data instead of just a single modality. Additionally, a single medical facility was the source of all patients in this study. By employing multi-center patient image data, the template will have greater universality. We will incorporate multi-center data in our future research endeavors.

Conclusion

All together, we created a CT brain template for patients with NPC in China. The generated CT brain template is the first one designed specifically for Chinese NPC patients in a conventional stereotaxic MNI space, and it can be utilized to concurrently spatially normalize planning CT and RTdose distribution map. Using the constructed CT brain template, we examined the group differences for various RTtechs of patients, and we discovered several intriguing variations from earlier reports: For NPC patients at the T4 stage, VMAT showed a drawback in preserving normal brain tissues. With better localization precision, we thought that the built MNI standard-space brain template in the CT modality could be very helpful for toxicity and dosimetric study of NPC patients.

Acknowledgements

This study was supported by the Zhejiang Provincial Basic Public Welfare Research Project (No. LGF22H160070) and the Medical Science and Technology Project of Zhejiang Provincial Health Commission (No. 2021-PY040).

Disclosure of conflict of interest

None.

Address correspondence to: Yonghong Hua, Department of Radiation Oncology, Zhejiang Cancer Hospital, Hangzhou Institute of Medicine (HIM), Chinese Academy of Sciences, Hangzhou 310022, Zhejiang, China. E-mail: huayh@zjcc.org.cn

References

[1] Chen YP, Chan ATC, Le QT, Blanchard P, Sun Y and Ma J. Nasopharyngeal carcinoma. Lancet 2019; 394: 64-80.

[2] Wong KCW, Hui EP, Lo KW, Lam WKJ, Johnson D, Li L, Tao Q, Chan KCA, To KF, King AD, Ma

BBY and Chan ATC. Nasopharyngeal carcinoma: an evolving paradigm. Nat Rev Clin Oncol 2021; 18: 679-695.
[3] Sun XS, Li XY, Chen QY, Tang LQ and Mai HQ. Future of radiotherapy in nasopharyngeal carcinoma. Br J Radiol 2019; 92: 20190209.
[4] Lee AW, Ma BB, Ng WT and Chan AT. Management of nasopharyngeal carcinoma: current practice and future perspective. J Clin Oncol 2015; 33: 3356-3364.
[5] Liu P, Niu X, Ou D, Qiu J, Lou P, Xue L, Zhou X, Xu T and Wang X. Dynamic changes in cognitive function in patients with radiation-induced temporal lobe necrosis after IMRT for nasopharyngeal cancer. Front Oncol 2020; 10: 450.
[6] Wang J, Miao Y, Ou X, Wang X, He X, Shen C, Ying H, Hu W and Hu C. Development and validation of a model for temporal lobe necrosis for nasopharyngeal carcinoma patients with intensity modulated radiation therapy. Radiat Oncol 2019; 14: 42.
[7] Hsiao KY, Yeh SA, Chang CC, Tsai PC, Wu JM and Gau JS. Cognitive function before and after intensity-modulated radiation therapy in patients with nasopharyngeal carcinoma: a prospective study. Int J Radiat Oncol Biol Phys 2010; 77: 722-726.
[8] Qiu Y, Guo Z, Han L, Yang Y, Li J, Liu S and Lv X. Network-level dysconnectivity in patients with nasopharyngeal carcinoma (NPC) early post-radiotherapy: longitudinal resting state fMRI study. Brain Imaging Behav 2018; 12: 1279-1289.
[9] Guo Z, Han L, Yang Y, He H, Li J, Chen H, Song T, Qiu Y and Lv X. Longitudinal brain structural alterations in patients with nasopharyngeal carcinoma early after radiotherapy. Neuroimage Clin 2018; 19: 252-259.
[10] Shi L, Du FL, Sun ZW, Zhang L, Chen YY, Xie TM, Li PJ, Huang S, Dong BQ and Zhang MM. Radiation-induced gray matter atrophy in patients with nasopharyngeal carcinoma after intensity modulated radiotherapy: a MRI magnetic resonance imaging voxel-based morphometry study. Quant Imaging Med Surg 2018; 8: 902-909.
[11] Lv X, He H, Yang Y, Han L, Guo Z, Chen H, Li J, Qiu Y and Xie C. Radiation-induced hippocampal atrophy in patients with nasopharyngeal carcinoma early after radiotherapy: a longitudinal MR-based hippocampal subfield analysis. Brain Imaging Behav 2019; 13: 1160-1171.
[12] McDowell LJ, Ringash J, Xu W, Chan B, Lu L, Waldron J, Rock K, So N, Huang SH, Giuliani M, Hope A, O'Sullivan B, Bratman SV, Cho J, Kim J, Jang R, Bayley A and Bernstein LJ. A cross sectional study in cognitive and neurobehavioral impairment in long-term nasopharyngeal cancer survivors treated with intensity-modulated radiotherapy. Radiother Oncol 2019; 131: 179-185.
[13] Mo YL, Li L, Qin L, Zhu XD, Qu S, Liang X and Wei ZJ. Cognitive function, mood, and sleep quality in patients treated with intensity - modulated radiation therapy for nasopharyngeal cancer: a prospective study. Psychooncology 2014; 23: 1185-1191.
[14] Palma G, Monti S and Cella L. Voxel-based analysis in radiation oncology: a methodological cookbook. Phys Med 2020; 69: 192-204.
[15] Fonov V, Evans AC, Botteron K, Almli CR, McKinstry RC and Collins DL; Brain Development Cooperative Group. Unbiased average age-appropriate atlases for pediatric studies. Neuroimage 2011; 54: 313-327.
[16] Xie W, Richards JE, Lei D, Zhu H, Lee K and Gong Q. The construction of MRI brain/head templates for Chinese children from 7 to 16 years of age. Dev Cogn Neurosci 2015; 15: 94-105.
[17] Tang Y, Hojatkashani C, Dinov ID, Sun B, Fan L, Lin X, Qi H, Hua X, Liu S and Toga AW. The construction of a Chinese MRI brain atlas: a morphometric comparison study between Chinese and Caucasian cohorts. Neuroimage 2010; 51: 33-41.
[18] Liu F, Zhang Z, Chen Y, Wei L, Xu Y, Li Z and Zhu C. MNI2CPC: a probabilistic cortex-to-scalp mapping for non-invasive brain stimulation targeting. Brain Stimul 2023; 16: 1733-1742.
[19] Germann J, Yang A, Chow CT, Santyr B, Samuel N, Vetkas A, Sarica C, Elias GJ, Voisin MR and Kucharczyk W. Review of template-based neuroimaging tools in neuro-oncology: novel insights. Onco 2022; 3: 1-12.
[20] Germann J, Zadeh G, Mansouri A, Kucharczyk W, Lozano AM and Boutet A. Untapped neuroimaging tools for neuro-oncology: connectomics and spatial transcriptomics. Cancers (Basel) 2022; 14: 464.
[21] Rorden C, Bonilha L, Fridriksson J, Bender B and Karnath HO. Age-specific CT and MRI templates for spatial normalization. Neuroimage 2012; 61: 957-965.
[22] Ghadimi S, Mohtasebi M, Abrishami Moghaddam H, Grebe R, Gity M and Wallois F. A neonatal bimodal MR-CT head template. PLoS One 2017; 12: e0166112.
[23] Rajashekar D, Wilms M, MacDonald ME, Ehrhardt J, Mouches P, Frayne R, Hill MD and Forkert ND. High-resolution T2-FLAIR and non-contrast CT brain atlas of the elderly. Sci Data 2020; 7: 56.
[24] Chilamkurthy S, Ghosh R, Tanamala S, Biviji M, Campeau NG, Venugopal VK, Mahajan V, Rao P and Warier P. Deep learning algorithms for detection of critical findings in head CT scans: a retrospective study. Lancet 2018; 392: 2388-2396.

[25] Muschelli J. A publicly available, high resolution, unbiased CT brain template. Information Processing and Management of Uncertainty in Knowledge-Based Systems: 18th International Conference, IPMU 2020, Lisbon, Portugal, June 15-19, 2020, Proceedings, Part III 18 2020; 358-366.
[26] Xie W, Richards JE, Lei D, Lee K and Gong Q. Comparison of the brain development trajectory between Chinese and US children and adolescents. Front Syst Neurosci 2015; 8: 249.
[27] Yang G, Zhou S, Bozek J, Dong HM, Han M, Zuo XN, Liu H and Gao JH. Sample sizes and population differences in brain template construction. Neuroimage 2020; 206: 116318.
[28] Tang Y, Zhao L, Lou Y, Shi Y, Fang R, Lin X, Liu S and Toga A. Brain structure differences between Chinese and Caucasian cohorts: a comprehensive morphometry study. Hum Brain Mapp 2018; 39: 2147-2155.
[29] Holla B, Taylor PA, Glen DR, Lee JA, Vaidya N, Mehta UM, Venkatasubramanian G, Pal PK, Saini J, Rao NP, Ahuja CK, Kuriyan R, Krishna M, Basu D, Kalyanram K, Chakrabarti A, Orfanos DP, Barker GJ, Cox RW, Schumann G, Bharath RD and Benegal V. A series of five population-specific Indian brain templates and atlases spanning ages 6-60 years. Hum Brain Mapp 2020; 41: 5164-5175.
[30] Bethesda M. ICRU Report 50: prescribing, recording, and reporting photon beam therapy. J ICRU 1993.
[31] Wambersie A. ICRU report 62, prescribing, recording and reporting photon beam therapy (supplement to ICRU Report 50). Icru News 1999.
[32] Units ICoR and Measurements. ICRU Report 83 Prescribing, Recording, and Reporting Photon-beam Intensity-modulated Radiation Therapy (IMRT)-Journal of the ICRU-Vol 10 No 1 2010. Oxford University Press; 2010.
[33] Lee N, Harris J, Garden AS, Straube W, Glisson B, Xia P, Bosch W, Morrison WH, Quivey J, Thorstad W, Jones C and Ang KK. Intensity-modulated radiation therapy with or without chemotherapy for nasopharyngeal carcinoma: radiation therapy oncology group phase II trial 0225. J Clin Oncol 2009; 27: 3684-90.
[34] Pauli WM, Nili AN and Tyszka JM. A high-resolution probabilistic in vivo atlas of human subcortical brain nuclei. Sci Data 2018; 5: 180063.
[35] Fedorov A, Beichel R, Kalpathy-Cramer J, Finet J, Fillion-Robin JC, Pujol S, Bauer C, Jennings D, Fennessy F, Sonka M, Buatti J, Aylward S, Miller JV, Pieper S and Kikinis R. 3D slicer as an image computing platform for the quantitative imaging network. Magn Reson Imaging 2012; 30: 1323-1341.
[36] Avants BB, Tustison NJ, Song G, Cook PA, Klein A and Gee JC. A reproducible evaluation of ANTs similarity metric performance in brain image registration. Neuroimage 2011; 54: 2033-2044.
[37] Yan CG, Wang XD, Zuo XN and Zang YF. DPABI: data processing & analysis for (resting-state) brain imaging. Neuroinformatics 2016; 14: 339-351.
[38] Xia M, Wang J and He Y. BrainNet viewer: a network visualization tool for human brain connectomics. PLoS One 2013; 8: e68910.
[39] Yao CY, Zhou GR, Wang LJ, Xu JH, Ye JJ, Zhang LF, He X, Chen ZZ and Huang SF. A retrospective dosimetry study of intensity-modulated radiotherapy for nasopharyngeal carcinoma: radiation-induced brainstem injury and dose-volume analysis. Radiat Oncol 2018; 13: 194.
[40] Fan X, Huang Y, Xu P, Min Y, Li J, Feng M, Xu G and Lang J. Dosimetric analysis of radiation-induced brainstem necrosis for nasopharyngeal carcinoma treated with IMRT. BMC Cancer 2022; 22: 178.
[41] Su SF, Huang Y, Xiao WW, Huang SM, Han F, Xie CM and Lu TX. Clinical and dosimetric characteristics of temporal lobe injury following intensity modulated radiotherapy of nasopharyngeal carcinoma. Radiother Oncol 2012; 104: 312-316.
[42] Qiu Y, Guo Z, Lin X, Li J, Li Z, Han L, Yang Y and Lv X. Standard radiotherapy for patients with nasopharyngeal carcinoma results in progressive tract-specific brain white matter alterations: a one-year follow-up via diffusion tensor imaging. Radiother Oncol 2021; 159: 255-264.
[43] Lin J, Lv X, Niu M, Liu L, Chen J, Xie F, Zhong M, Qiu S, Li L and Huang R. Radiation-induced abnormal cortical thickness in patients with nasopharyngeal carcinoma after radiotherapy. Neuroimage Clin 2017; 14: 610-621.
[44] Lu SH, Cheng JC, Kuo SH, Lee JJ, Chen LH, Wu JK, Chen YH, Chen WY, Wen SY, Chong FC, Wu CJ and Wang CW. Volumetric modulated arc therapy for nasopharyngeal carcinoma: a dosimetric comparison with TomoTherapy and step-and-shoot IMRT. Radiother Oncol 2012; 104: 324-330.
[45] He L, Xiao J, Wei Z, He Y, Wang J, Guan H, Mu X and Peng X. Toxicity and dosimetric analysis of nasopharyngeal carcinoma patients undergoing radiotherapy with IMRT or VMAT: a regional center's experience. Oral Oncol 2020; 109: 104978.
[46] Chen BB, Huang SM, Xiao WW, Sun WZ, Liu MZ, Lu TX, Deng XW and Han F. Prospective matched study on comparison of volumetric-modulated arc therapy and intensity-modulated radiotherapy for nasopharyngeal carcinoma: dosimetry, delivery efficiency and outcomes. J Cancer 2018; 9: 978-986.

Supplementary File: The detailed sub-brain regions

Average of RTdose images

The overview of RTdose images was derived by averaging patients' RTdose images for each RTtech of patients. The RTdose images were projected into the Colin27 MRI brain surface template in BrainNet viewer toolbox(38). To illustrate the brain regions accepted relatively higher dose during RT, regions that covered by the > 30 Gy and > 50 Gy dose distribution maps were also illustrated. The schematic diagram was shown in **Figure 2**.

To illustrate the regions accepted relatively higher dose during RT, locations of brain regions that covered by the > 50 Gy dose distribution map of patients were reported, shown in **Table 2**. Brain regions that covered by the > 50 Gy dose distribution map of patients treated by the IMRT RTtech included part of the Limbic Lobe (including part of the Uncus), the Temporal Lobe (including part of the Inferior Temporal Gyrus, the Superior and Middle Temporal Gyrus, and a bit of the Sub-Gyral), the Brainstem (including part of the Pons and Medulla), and part of Cerebellum Posterior Lobe (including part of the Cerebellar Tonsil). Brain regions that covered by the > 50 Gy dose distribution map of patients treated by the VMAT RTtech included part of the Limbic Lobe (including part of the Uncus), the Temporal Lobe (including part of the Superior Temporal Gyrus, the Inferior and Middle Temporal Gyrus, and a bit of the Sub-Gyral), the Brainstem (including part of the Pons and Medulla), and part of Cerebellum Posterior Lobe (including part of the Cerebellar Tonsil). The result showed that brain regions covered by the > 50 Gy dose distribution map of patients treated by IMRT and VMAT were very similar.

Differences in RTdose images between IMRT and VMAT RTtechs

Group differences in RTdose data for different RTtechs of all patients were shown in **Figure 3A**. The detailed brain regions of the group differences were executed by xjView toolbox.

Brain regions in which the delivered dose was significantly lower in patients treated with the IMRT method than that with VMAT were located in part of the Cerebellum Posterior Lobe (including part of the Declive, the Cerebellar Tonsil, the Inferior Semi-Lunar Lobule, the Pyramis, the Uvula, the Tuber, the Uvula of Vermis, the pyramis of Vermis, and the Declive of Vermis), the Occipital Lobe (including part of the Middle Occipital Gyrus, the Lingual Gyrus, the Fusiform Gyrus, the Inferior Occipital Gyrus, the Sub Gyral and a bit of the Cuneus), the Cerebellum Anterior Lobe (including part of the Culmen, most of the Dentate, the Nodule and the Fastigium), the Temporal Lobe (including part of the Inferior Temporal Gyrus, The Middle Temporal Gyrus, the Fusiform Gyrus, and a bit of the Sub Gyral), the Brainstem (including part of the Medulla and the Pons), the Frontal lobe (including part of the of the Sub Gyral, the Medial Frontal Gyrus, the Inferior, Middle and Superior Frontal Gyrus, and the Precentral Gyrus), the Sub Lobar (including most of the Fourth Ventricle, part of the Extra-Nuclear, the Insula, the Lateral Ventricle, the Caudate, the Lentiform nucleus and the Claustrum), and the Limic lobe (including part of the Anterior Cingulate, and the Cingulate Gyrus).

Brain regions in which the delivered dose was significantly higher in patients treated with the IMRT method than that with VMAT were located in part of the Temporal lobe (including part of the Superior Temporal Gyrus, the Middle Temporal Gyrus, part of the Sub Gyral, the Inferior Temporal Gyrus, and a bit of the Fusiform Gyrus), the Frontal Lobe (including part of the Inferior Frontal Gyrus, most of the Rectal Gyrus and the Medial Frontal Gyrus, a little part of the Sub Gyral, the Subcallosal Gyrus, the Orbital Gyrus and the Middle Frontal Gyrus), the Limbic Lobe (including part of the Parahippocampal Gyrus, the Uncus, the Amygdala and a bit of the Anterior Cingulate), the Brainstem (including part of the Midbrain, a bit of the Pons and the Substania Nigra), a little part of the Sub Lobar (including a bit of the Extra Nuclear, the Lateral Ventricle, and the Third Ventricle), a bit of the Cerebellum Anterior Lobe (including a little part of the Culmen), and part of the Occipital Lobe (including part of the Cuneus).

Voxel sizes, peak T values and locations of the peak value in MNI space for each brain regions described above were depicted in **Table 3**.

No significant difference was detected in RTdose data for different RTtechs of T1 patients.

Group differences in RTdose data for different RTtechs of T2 stage patients were shown in **Figure 3B**. The detailed brain regions of the group differences were executed by xjView toolbox.

Brain regions in which the delivered dose was significantly higher in patients treated with the IMRT method than that with VMAT were located in a part of the Frontal Lobe (including part of the Middle Frontal Gyrus, the Superior Frontal Gyrus, the Medial Frontal Gyrus, the Inferior Frontal Gyrus, the Precentral Gyrus, the Paracentral Lobule, most of the Rectal Gyrus, the Subcallosal Gyrus, and the Orbital Gyrus), the Temporal Lobe (including part of the Sub Gyral, the Middle Temporal Gyrus, the Superior Temporal Gyrus, the Inferior Temporal Gyrus, and the Fusiform Gyrus), the Parietal Lobe (including part of the Postcentral Gyrus, the Precuneus, the Inferior Parietal Lobule, the Superior Parietal Lobule, and a bit of the Supramarginal Gyrus), the Limbic Lobe (including part of the Cingulate Gyrus, the Parahippocampal Gyrus, the Uncus, and a bit of the Anterior Cingulate and the Posterior Cingulate), the Brainstem (including part of the Midbrain and the Pons), a bit of the Sub Lobar (including a bit of the Extra Nuclear, the Lateral Ventricle, the Lentiform Nucleus, Thalamus, Insula and the Third Ventricle), and a bit of the Cerebellum Anterior Lobe including (a bit of the Culmen).

Brain regions in which the delivered dose was significantly lower in patients treated with the IMRT method than that with VMAT were located in a part of the Cerebellum Posterior Lobe (including part of the Inferior Semi-Lunar Lobule, the Cerebellar Tonsil, the Pyramis, the Uvula, the Tuber, and the Uvula of Vermis), and a bit of the Brainstem (including a little part of the Medulla).

Voxel sizes, peak T values and locations of the peak value in MNI space for each brain regions described above were depicted in Table S1.

Group differences in RTdose data for different RTtechs of T3 stage patients were shown in **Figure 3C**. The detailed brain regions of the group differences were executed by xjView toolbox.

Brain regions in which the delivered dose was significantly higher in patients treated with the IMRT method than that with VMAT were located in a part of the Temporal Lobe (including part of the Superior Temporal Gyrus, the Middle Temporal Gyrus, a little part of the Sub Gyral and the Inferior Temporal Gyrus, and a bit of the Fusiform Gyrus), the Frontal Lobe (including part of the Inferior Frontal Gyrus, the Rectal Gyrus, the Subcallosal Gyrus, the Medial Frontal Gyrus, the Orbital Gyrus, and a bit of the Middle Frontal Gyrus), the Limbic Lobe (including part of the Parahippocampa Gyrus, the Uncus, and the Posterior Cingulate), the Occipital Lobe (including part of the Cuneus, the Middle Occipital Gyrus, the Lingual Gyrus and the Precuneus), the Brainstem (including part of the Midbrain and the Pons), the Sub Lobar (including part of the Extra-Nuclear, Lateral Ventricle and the Third Ventricle), a bit of the Cerebellum Anterior Lobe (including part of the Culmen).

Brain regions in which the delivered dose was significantly lower in patients treated with the IMRT method than that with VMAT were located in a part of Cerebellum Posterior Lobe (including part of the Declive, the Pyramis, the uvula, the inferior Semi-Lunar Lobule, the Cerebellar Tonsil, and the Tuber), the Occipital Lobe (including part of the Inferior Occipital Gyrus, the Fusiform Gyrus, the Lingual Gyrus and the Middle Occipital Gyrus), the Cerebellum Anterior Lobe (including part of the Dentate, the Nodule, the Uvula of Vermis and the Culmen), and the Brainstem (including part of the Medulla).

Voxel sizes, peak values and locations of the peak value in MNI space for each brain regions described above were depicted in Table S2.

Group differences in RTdose data for different RTtechs of T4 stage patients were shown in **Figure 3D**. The detailed brain regions of the group differences were executed by xjView toolbox.

No brain regions in which the delivered dose was significantly higher in patients treated with the IMRT method than that with VMAT were found. Brain regions in which the delivered dose was significantly lower in patients treated with the IMRT method than that with VMAT were located in a part of the Cerebellum Posterior Lobe (including part of the Declive, the Cerebellar Tonsil, the Inferior Semi-Lunar Lobule, the Pyramis, the Uvula, the Tuber and the Uvula of Vermis), the Occipital Lobe (including part the Fusiform Gyrus, the Middle Occipital Gyrus, the Inferior Occipital Gyrus, the Lingual Gyrus, and a bit of the Cuneus), the Cerebellum Anterior Lobe (including part of the Culmen, the Dentate, the Nodule and the Fastigium), the Temporal Lobe (including a little part of the Sub Gyral, the Inferior Temporal Gyrus, and the Middle Temporal Gyrus), the Frontal lobe (including part of the Sub Gyral, the Medial Frontal Gyrus, the Superior Frontal Gyrus, the Middle Frontal Gyrus, the Inferior Frontal Gyrus and a bit of the Precentral Gyrus), the Brainstem (including part of the Pons, the Medulla and Midbrain), the Limbic Lobe (including part of the Parahippocampa Gyrus, the Anterior Cingulate, and a bit of the Uncus), and the Sub Lobar (including part of the Fourth Ventricle, part of the Extra-Nuclear, the Insula, the Corpus Callosum, a bit of the Lateral Ventricle and the Claustrum).

Voxel sizes, peak values and locations of the peak values in MNI space for each brain regions described above were depicted in Table S3.

Table S1. Brain regions showed significant differences in RTdose images between RTtechs (IMRT vs. VMAT) in T2 patients in a two-sample t-test by using a permutation threshold-free cluster enhancement test (number of permutations = 5000, FWE P < 0.05), sample size: 2*2*2, voxel size > 30

Regions	Voxel size	Peak T value	MNI coordinate		
			x	y	z
IMRT < VMAT					
Cerebellum Posterior Lobe	1405	-6.42	2	-56	-50
Medulla	48	-6.03	2	-48	-52
IMRT > VMAT					
Frontal Lobe	37246	7.09	22	14	-26
Temporal Lobe	10594	7.06	224	12	-26
Parietal Lobe	5950	4.62	68	-18	36
Limbic Lobe	7499	6.95	26	10	-26
Midbrain	2013	6.74	4	-10	-22
Sub-lobar	1788	6.33	-22	-6	-24
Pons	736	6.66	2	-12	-24
Cerebellum Anterior Lobe	324	3.65	14	-28	-18

IMRT: Intensity-modulated radiotherapy; VMAT: Volumetric Modulated Arc Therapy; RTtechs: radiotherapy technicals; MNI: Montreal Neurological Institute; FWE: family-wise error.

Table S2. Brain regions showed significant differences in RTdose images between RTtechs (IMRT vs. VMAT) in T3 patients in a two-sample t-test by using a permutation threshold-free cluster enhancement test (number of permutations = 5000, FWE $P < 0.05$), sample size: 2*2*2, voxel size > 30

Regions	Voxel size	Peak T value	MNI coordinate		
			x	y	z
IMRT < VMAT					
Cerebellum Posterior Lobe	5342	-9.24	2	-54	-50
Occipital Lobe	1007	-5.57	22	-94	-26
Cerebellum Anterior Lobe	209	-5.46	20	-66	-34
Medulla	160	-8.48	2	-48	-52
IMRT > VMAT					
Temporal Lobe	5593	7.89	30	14	-24
Frontal Lobe	3236	7.90	30	16	-24
Limbic Lobe	2208	8.39	12	0	-22
Midbrain	1594	7.95	6	-10	-20
Occipital Lobe	1760	4.05	2	-96	18
Pons	233	6.95	-6	-10	-24
Cerebellum Anterior Lobe	312	3.68	12	-32	-14
Sub-lobar	649	6.28	-22	-6	-24

IMRT: Intensity-modulated radiotherapy; VMAT: Volumetric Modulated Arc Therapy; RTtechs: radiotherapy technicals; MNI: Montreal Neurological Institute; FWE: family-wise error.

Table S3. Brain regions showed significant differences in RTdose images between RTtechs (IMRT vs. VMAT) in T4 patients in a two-sample t-test by using a permutation threshold-free cluster enhancement test (number of permutations = 5000, FWE $P < 0.05$), sample size: 2*2*2, voxel size > 30

Regions	Voxel size	Peak T value	MNI coordinate		
			x	y	z
IMRT < VMAT					
Cerebellum Posterior Lobe	8085	-8.66	2	-50	-50
Occipital Lobe	3454	-5.90	-26	-2	-26
Frontal Lobe	2266	-3.82	-18	42	0
Cerebellum Anterior Lobe	2395	-6.03	-2	-40	-34
Temporal Lobe	2323	-7.14	-58	-54	-24
Pons	1345	-6.51	0	-44	-42
Limbic Lobe	1010	-4.13	-40	-32	-26
Sub-lobar	1169	-7.23	0	-50	-44
Medulla	452	-8.54	2	-48	-50
Midbrain	32	-3.47	0	-38	-24
IMRT > VMAT					
None					

IMRT: Intensity-modulated radiotherapy; VMAT: Volumetric Modulated Arc Therapy; RTtechs: radiotherapy technicals; MNI: Montreal Neurological Institute; FWE: family-wise error.